Optik - International Journal for Light and Electron Optics 265 (2022) 169418

Contents lists available at ScienceDirect

Optik

journal homepage: www.elsevier.com/locate/ijleo

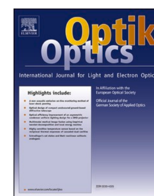

Original research article

# Fabrication of GaN nanocrystalline thin films Schottky metal-semiconductor-metal ultraviolet photodetectors

Abbas M. Selman [a,b,*], M.J. Kadhim [c]

[a] Department of Pharmacognosy and Medicinal plants, Faculty of Pharmacy, University of Kufa, Najaf, Iraq
[b] Institute of Nano Optoelectronics Research and Technology (INOR), Universiti Sains Malaysia (USM), Penang 11800, Malaysia
[c] Department of Chemistry, College of Science, University of Basrah, Basrah, Iraq

ARTICLE INFO

*Keywords:*
GaN
Nanoparticles
Detectivity
Nanocrystalline
Schottky MSM

ABSTRACT

Gallium nitride nanocrystalline thin films (GaN NCTH) were prepared on Si substrates using the radio frequency magnetron sputtering (RF) method. XRD patterns with narrow peaks intensity and field emission scanning electron microscopy (FESEM) images exhibits of the GaN nanoparticles have covered surfaces of the substrate with a regular distribution smooth and an average particles size proximately between are 10–20 nm. AFM indicates a smooth surface and RMS is 1.38 nm of GaN NCTH and the optical band gap was calculated to be 3.38 eV. The current-voltage characteristic of metal-semiconductor-metal (M-S-M) GaN ultraviolet photodetectors (UV-PD) in the dark and irradiated with 370 nm light and intensity was (1.4) mW/cm$^2$ evaluated under bias voltages of −1 to 5 V. The average rise time speed of the photodetector is about 22 ms when current increases from 10 % to 90 % of its value of saturation, while the average fall time is 17 ms when current decreases from 90 % to 10 % of its value of saturation. UV-PD displays 19–261 sensitivity at a different voltage bias; internal photodetector gain between the low value is 1.19 at 8 V and 1.59 at 2 V.

## 1. Introduction

Gallium Nitride (GaN) is a semiconducting and one of the most committed materials and has a broad bandgap direct [1,2] is between (3.2–3.4) eV based on the structure of the crystal [3]. Moreover, GaN possesses properties of which non-toxic [4], excellent chemically [5], thermally stable, and thermal conductivity [6] and have a peak of high extremely is (3 × 10$^7$ cm s$^{-1}$), a very high voltage breakdown (3 × 10$^6$ Vcm$^{-1}$), and velocity of saturation (1.5 ×10$^7$ cm s$^{-1}$) [7], resistant (inert) in environments of extreme such as radioactive [8], and a high optical transition probability, making it a perfect building block for optoelectronic systems that use blue-green light-emitting diodes, laser diodes, and other choice materials [6]. GaN thin film prepared was by several techniques, such as chemical vapor deposition (CVD) [9], RF, sol-gel [10], hydride vapor phase epitaxy [11], and molecular beam epitaxy [12]. Although the quality of GaN thin films is good, the manufacturing cost prepared by the methods mentioned is relatively high, difficult to handle in air, and the setup is complicated [13]. It is used in the synthesis of many important applications of devices such as transistors of high power [14], solar cell [15], betavoltaic [16], photodetector [17], and light-emitting diode (LED) devices [18]. As stated above, GaN nanoparticles are known to have good luminous centers, which refers to the effect of quantum confinement. Thus, quantum dots electronic structure formation of well separated atomic like states with increases in energy spacing as dot size decreases.

* Corresponding author at: Department of Pharmacognosy and Medicinal plants, Faculty of Pharmacy, University of Kufa, Najaf, Iraq.
*E-mail addresses:* bbasm.salman@uokufa.edu.iq, alabbasiabbas@yahoo.co.uk (A.M. Selman).

https://doi.org/10.1016/j.ijleo.2022.169418
Received 5 April 2022; Received in revised form 23 May 2022; Accepted 30 May 2022
Available online 4 June 2022
0030-4026/© 2022 Elsevier GmbH. All rights reserved.

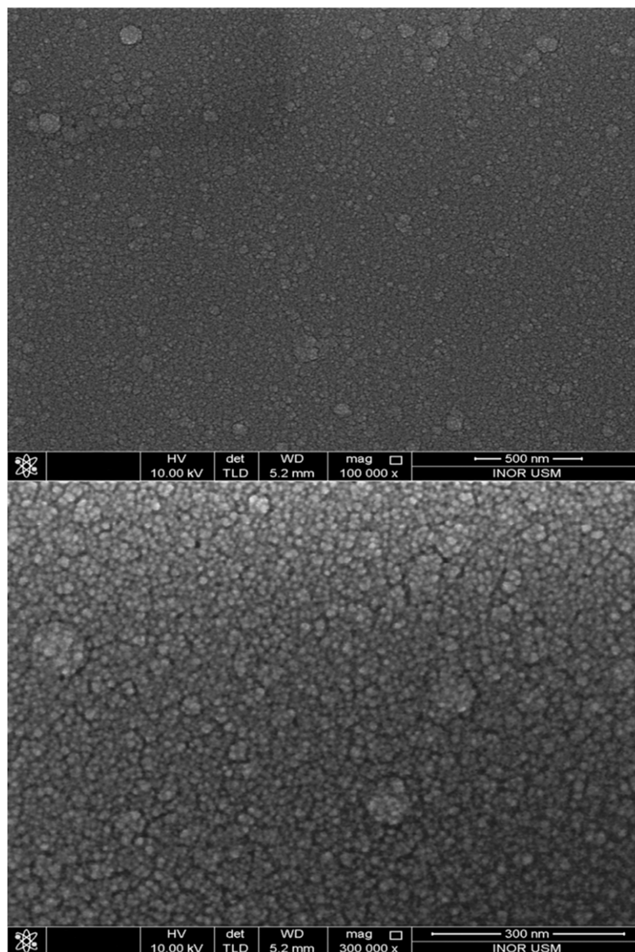


**Fig. 1.** FESEM image of GaN NCTH prepared on Si substrate.

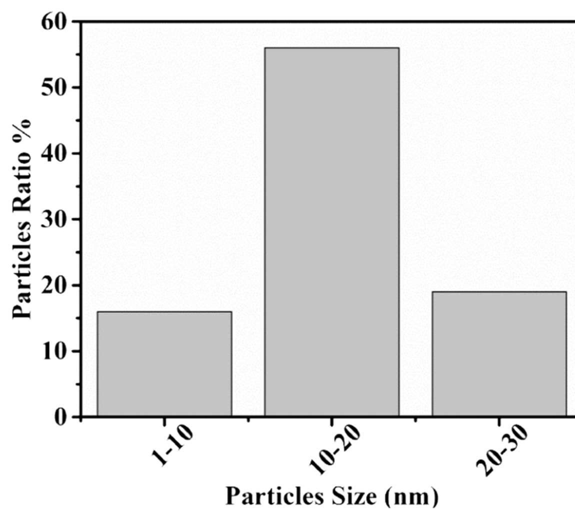


**Fig. 2.** Statistical distribution of particles size of GaN NCTH prepared on Si substrate.

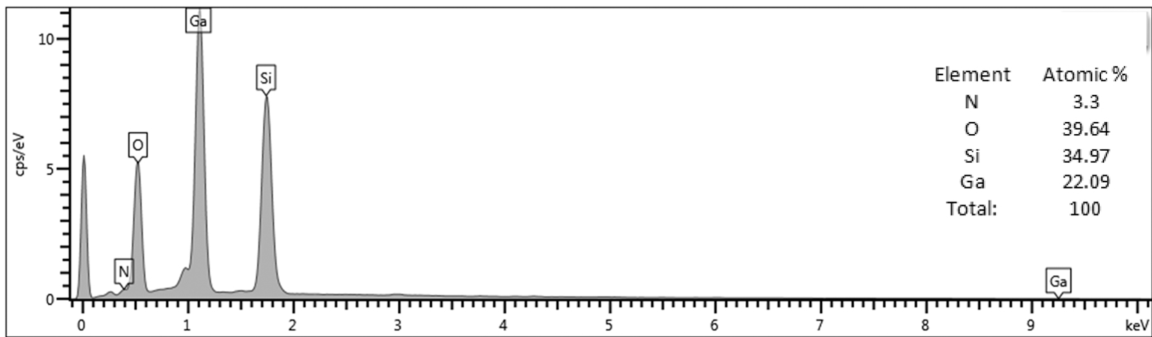


**Fig. 3.** The EDX spectra results of GaN NCTH prepared on Si substrate.

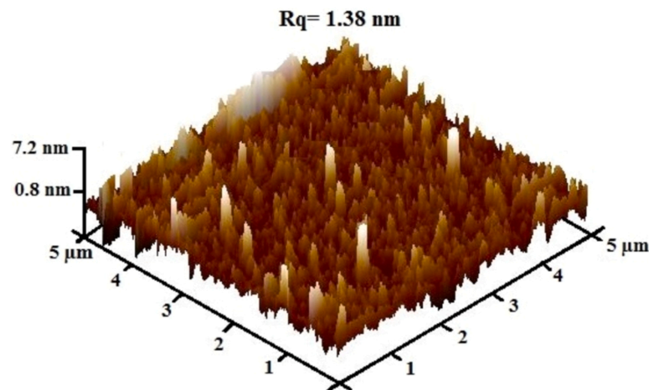


**Fig. 4.** AFM 3D micrograph of GaN NCTH prepared on Si substrate.

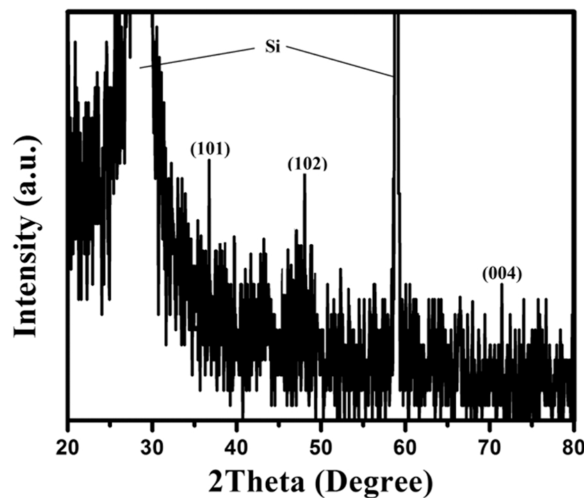


**Fig. 5.** XRD patterns of GaN NCTH prepared on Si substrate.

Hence, the mixing quantum dot size properly chosen leads to the emission of white light [19]. In this study, a field emission scanning electron microscope (FESEM) was used to explore the surface morphology. Meanwhile, an atomic force microscope (AFM) was used to measure the roughness of the surface. High-resolution X-ray diffractometry (HRXRD) was used to study the structures. Finally, a Raman scattering spectroscopy device was used to offer a structural fingerprint that can be used to identify compounds.

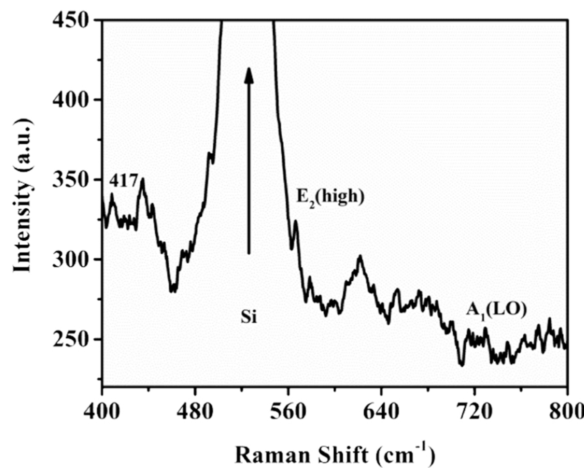


**Fig. 6.** Raman spectra of GaN NCTH prepared on Si substrate.

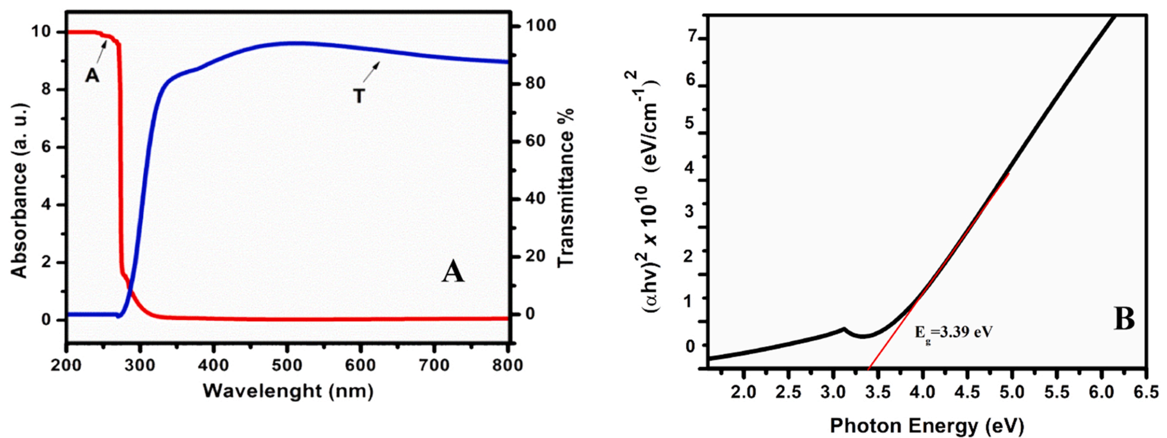


**Fig. 7.** (A) UV–vis spectra for GaN NCTHs prepared on Si substrates (B) A plot of $(\alpha\, h\nu)^2$ versus $(h\nu)$.

### 1.1. Experimental details

As described in previous work [20] synthesis of GaN NCTH on P-type Si (111) substrate, was preceded by cleaning of Si substrates using the RCA method with chemical wet etching [21], (we added cleaned glass substrates to deposition same films for optical studies purpose) and then NCTH deposited by RF method through 80 min recorded times of growth (200 ± 5) nm.

## 2. Results and discussion

### 2.1. Morphological and structural characterizations of GaN NCTH

Fig. 1 exhibits a FESEM image of GaN NCTH prepared on Si substrate with 300 and 500 nm magnification. These images show a homogeneous distribution of aggregated to form grains with an average particles size are (10−20) nm according to the image-j program as noted in Fig. 2. EDX analysis was also used to determine the GaN NCTH prepared on Si, as shown in Fig. 3, which appears to have a Ga to N ratio in GaN thin films and noted oxygen atoms, perhaps present as a result of surface contaminants spreading from the substrate during the deposition process. [22]. Moreover, topography AFM indicates a smooth surface and the RMS of GaN NCTH prepared on Si is 1.38 nm as shown in Fig. 4, while Mantarcl and Kundakçi referred to RMS of 6.257 and 1.024 nm of GaN/Si synthesized by the RF method [23]. However, Thahab reported the RMS of n-type and p-type GaN/Si obtained were 14.8 and 4.37, respectively [24]. As a matter of fact, a previous study referred to substrate type having an affected roughness surface, which referred to RMS GaN NCTH prepared on quartz, glass, and FTO were (1.46, 1.45, and 30.8) nm, respectively [1]. Fig. 5 exhibits XRD analysis associated with GaN NCTH with a narrow peak at three plans (101), (102), and (004) corresponding to 2 Theta (36.9, 48, and 72,6) degrees [22,25–29]. Meanwhile, XRD exhibits two peaks related to Si substrate at plans (111) and (222), corresponding to (28.25, and 58.87) degrees, respectively, according to database 01–077–2111.

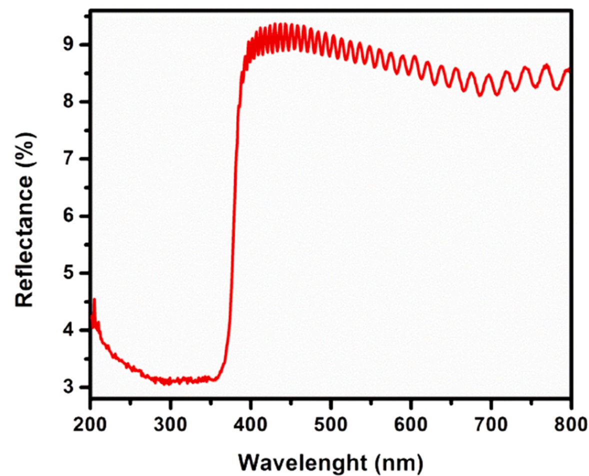


**Fig. 8.** Reflectance spectra of GaN NCTH prepared onto Si substrates.

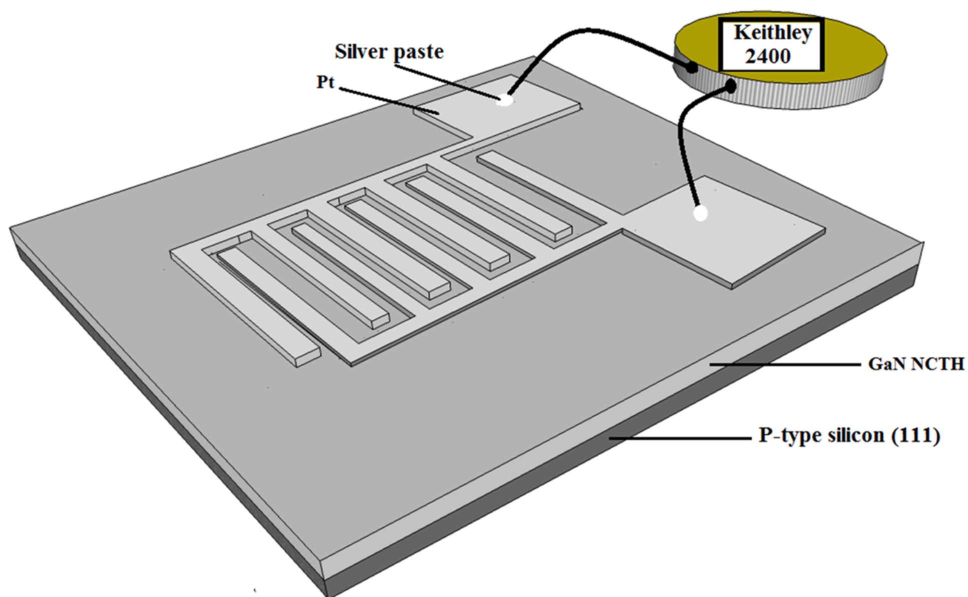


**Fig. 9.** The schematic diagram of the device (GaN NCTH MSM UV-PD).

### 2.2. Raman and optical properties

Raman scattering spectroscopy of the GaN NCTH on Si substrate samples is shown in Fig. 6. As shown in Raman spectra exhibit one, a clear high-intensity peak returns to Si at 520 $cm^{-1}$ and the noted active phonon $E_2$(high) band returns to GaN at 566 $cm^{-1}$ while $A_1$(LO) is 730 $cm^{-1}$ and these bands correspond to previous [30,31]. Two phonon $E_2$(high) and $A_1$(LO) in GaN corresponded to backscattering. However, in undoped material, the intensity ratio band $A_1$(LO) to $E_2$(high) is relative to 1:3 [30]. Saron et al. reported a position intensity band related to the temperature of preparation, which was an inverse [32]. At 417 $cm^{-1}$, it exhibits a small peak return phonon mode which, means the acoustic overtone mode in GaN wurtzite [32]. Fig. 7A exhibits optical properties for GaN NCTH, which have a noted optical absorption spectrum and appear to have a strong edge of absorption present at a wavelength of 320 nm. The transmission spectra exhibit a high transmission in the visible region between 85 % and 90 % while Bittar et al. reported a transmission value is 60 % of GaN prepared on Si substrate [33]. The Energy of the bandgap is calculated from the relationship $\alpha h\nu = A(h\nu - E_g)^{1/2}$ [34], where , $h\nu$, $\alpha$, and $E_g$ are constant, photon energy, absorption coefficient, and bandgap, respectively. Therefore, absorbtion coefficient was relationship of transmation T according to equation $\alpha = \frac{1}{d}\ln\,(1/T)$ [35] where (d) is the thickness of the thin film. Assuming bandgap direct as shown in Fig. 7(B) and estimated bandgap of GaN NCTH is 3.39 eV, which matches the value obtained by Duanet et al. [36]. While El-Naggar reported to a bandgap of GaN prepared on Si are (3.33–3.35) eV and refer to the bandgap

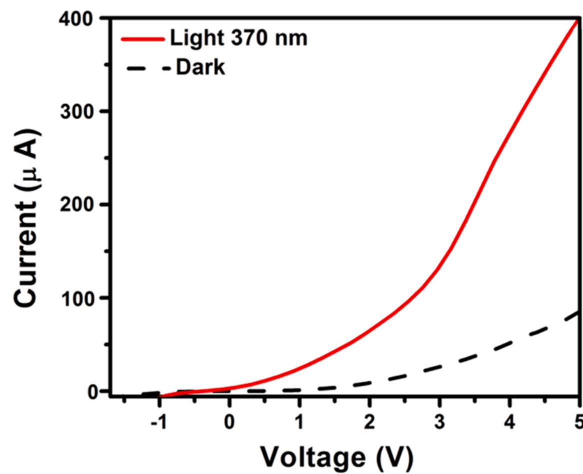


**Fig. 10.** I-V characteristic of M-S-M GaN prepared on Si photodetector in dark and irradiation.

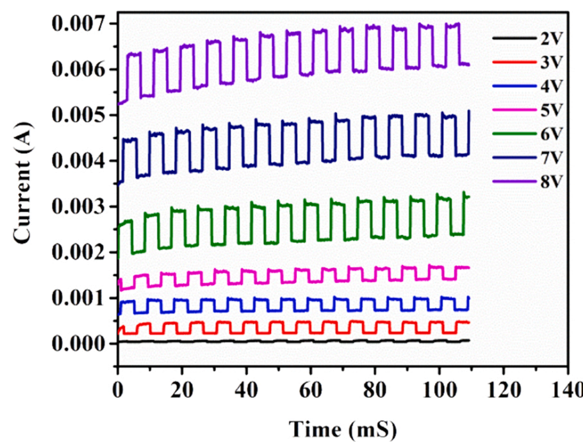


**Fig. 11.** Response time of M-S-M GaN prepared on Si photodetector irradiation by chopped 370 nm.

depending on a precise ratio of ionic and covalence bonds in GaN of the structure band determined and energy of such compounds type [37]. Fig. 8 exhibits the reflectance spectrum of the prepared GaN NCTH, which has low reflectance values in visible spectrum, 9 % a reflectance value in the wavelengths ranging 380–450 nm. Refer low reflectance the more UV photodetectors absorbed, which means the photo sensitivity (S) of increasing [38].

### *2.3. Device fabrication*

The MSM-structured UV-PD device was produced by depositing a Pt grid (100 nm thickness) on top of GaN NCTH using a metal mask. Previous work [39] illustrates the dimensions and design of the shadow mask. The deposition process of Pt electrodes using RF reactive magnetron sputtering was carried out under the following conditions: chamber vacuum of $2 \times 10^{-5}$ mbar, high-purity argon (99.99 %) as sputtering gas at a 17 % fixed ratio, a total pressure of $3 \times 10^{-3}$ mbar with an RF power of 120 W and a temperature of 25 °C. Fig. 9 displays the schematic design of MSM UV-PD for measuring the photocurrent. The device's effective area is 0.1634 $cm^2$ and was estimated using the area of the GaN NCTH sample exposed to light without Pt electrodes. The same value was determined by our prior study [39].

Fig. 10 illustrates the I-V characteristics of fabricated M-S-M GaN PD under dark and illumination by 1.4 $mW/cm^2$ intensity of 370 nm light. The photodetector exhibits the Schottky behavior of nonlinear and increased current with increases in applied voltage. The Schottky contact obtains deposited Pt-metal onto n-GaN because the value of work function Pt ($\phi_m$) is 5.65 eV and the value of electron affinity GaN ($\chi$) is 4.1 eV. The value of ideal barrier height ($\phi_B$) onto n-type GaN is 1.55 eV can be computed by assuming the nonappearance (theoretically) of interface states [40].

The generated current of the photodetector was measured at a range of bias voltages applied from −1–5 V on the contacts. The average rise time speed of the photodetector is about 22 ms when the current increases from 10 % to 90 % of its value of saturation,

**Table 1**
Comparison of the photoelectrical factors of variation GaN UV-PD.

| Bais Voltage V | GaN Nanost. | λ nm | S% | $I_{Ph}$ A | R A/W | D Jones | $\eta$ | Ref. |
|---|---|---|---|---|---|---|---|---|
| 2 | NPs | 370 | 60 | 0.000067 | 0.293 | $8.8 \times 10^{21}$ | 1 | This work |
| 3 | | | 261 | 0.00033 | 1.442 | $1.9 \times 10^{22}$ | 5 | |
| 4 | | | 125 | 0.00045 | 1.967 | $1.2 \times 10^{22}$ | 7 | |
| 5 | | | 36 | 0.0015 | 6.556 | $1.3 \times 10^{22}$ | 22 | |
| 1 | NFs | 325 | – | $113.6 \times 10^{-6}$ | 10.5 | $2.4 \times 10^{10}$ | – | [53] |
| 5 | NWs | 360 | – | $10^{-10}$ | 0.5 | – | – | [54] |
| 0 | – | – | – | $3.53 \times 10^{-11}$ | 0.03 | $1.8 \times 10^{12}$ | – | [55] |
| 10 | – | – | – | – | 3.096 | – | – | [47] |

while the average fall time is 17 ms when the current decreases from 90 % to 10 % of its value of saturation. Wang et al. [41] reported rise time of GaN PD is 70 ms and the fall time is 90 ms but reported of shorter response time (rise time <10 ms and fall time <10 ms) at Si-doped devices. While Krishna et al. [42] refer rise time between (23−117) ms and fall time between (16−56) ms.

When the photodetector is exposed to light, photocurrent is produced, which increases the overall amount of current by creating electron-hole pairs. Thus, because the detector is usually built to detect a specific wavelength or range of wavelengths, studying the photosensor's photoresponse can help determine the sensor's response peak [43]. Returning to Fig. 10, notice how the ohmic behaver at the Pt electrode deposition contact with GaN NCTH while the Schottky behaver Al metal contact with the device. However, contact type depends on the woke function of metal and semiconductors. In the case of ohmic contact, the work function of the metal is smaller than that of semiconductor n-type, while in the state of p-type semiconductors, the opposite is true. [43].

Fig. 11 exhibits the response time of M-S-M GaN UV-PD irradiation by chopped 370 nm UV light with 1.6 mW/$cm^2$ under (2−8) bias voltages. These curves exhibit figures of rectangular shape and agreeable variation with time under UV light irradiation when on and off switched repeatedly. Nonetheless, the photocurrent for every cycle on and off is steady and repeatable. In addition, the sensitivity (S) of the M-S-M GaN PD was determined by using relation ($S(\%) = \frac{I_{ph}-I_d}{I_d} \times 100$) at a different applied bias voltage [44]. Where $I_{ph}$, and $I_d$ are photocurrent and dark current, respectively, the sensitivity S (%) of UV-PD at 3 V is the highest (261), while the lowest value is 19 at 8 V. Prakash et al. reported sensitivity of GaN photodetector with 350 nm is 5.3 % at 0.2 V is less than 16 times compared to the sensitivity of r-GO/GaN photodetector [45]. The responsitivity (R) was evaluated for the photodetector and indicates the ratio of photocurrent to incident light power density (E) on the device's effective active area (A) [45] which is represented by the relation $R = I_{Ph}(A)/[E(W/cm^2) \times A(cm^2)]$ [46]. At this wave length and bias voltage 8 V gain of high value responsivity is 27.972 A/W while Cange et al. [47] calculated the responsitivity at 10 V which, is less than this work, and was 3.096, 1.079, and 2.420 A/W. The reason for the less value of photoresponse is due to the increase in light intensity and also increases the of recombination possibility according to previous literature [48,49]. Meanwhile, quantum efficiency ($\eta$) and detectivity (D) are significant factors in the assessment of a photosensitive device's performance, so quantum efficiency is given by the equation and is related to the number of charge carrier pairs excited by absorbed photons, and it is represented by $\eta = hcR/e\lambda$ [50]. As shown in the following relation, the detectivity of a photodetector is defined as the lowest level at which it can respond. $D = \frac{R\sqrt{A}}{\sqrt{2eI_d}}$ [45], where e, $\lambda$, h, and c are the electric charge, wavelength of UV light, Plank's constant, and speed of light, respectively. High value of detectivetiy is $2.4 \times 10^{23}$ Jones at 8 V of the GaN NCTH UV-PD while Nallabala et al. [51] reported detectivity of $9.4 \times 10^{14}$ Jones of the Au/$Nd_2O_3$/GaN MIS BB PD hypered device. In addation yadav et al. [52] reported D value is $1.73 \times 10^{13}$ Jones of the ITO/GaN/ITO. In this paper, the ratio value of photocurrent to darkcurrent was studied, which is known as gain (g) where gain the low value are 1.59, 1.26, 1.13, 1.36, 1.38, 1.25, and 1.19 at 2, 3, 4, 5, 6, 7 and 8 V respectively. Table 1 summarizes the photoelectrical properties of the GaN NCTH UV-PD and compares it with other GaN UV-PD devices fabricated.

## 3. Conclusions

GaN NCTH prepared on the Si substrate was synthesized by RF method. GaN NCTH is nanoparticles that show morphology formation and particle size of GaN NCTH ranging from 10 to 20 nm. XRD patterns show that the synthesis of thin films is polycrystalline. Hence, the XRD patterns of GaN NCTH which shows a characteristic peak at plans (101), (102), and (004) are corresponding to 2 Theta (36.9, 48, and 72,6) degree while XRD patterns Si in (111), and (222) corresponding to (28.25, and 58.87) degrees, respectively. On the other hand, Raman spectra exhibit one a clear high-intensity peak returns to Si at 520 $cm^{-1}$ and noted active phonon $E_2$(high) band returns GaN at 566 $cm^{-1}$ while $A_1$(LO) is 730 $cm^{-1}$ and these bands correspond to previous. The UV-PD appears of resulted in responsivity high at 8 V applied bias under 370 nm of irradiation of (1.6) mW/$cm^2$ light intensity which indicates results that the UV detector shows excellent stability over time, good sensitivity, and high photocurrent.

## Declaration of Competing Interest

The authors declare that they have no known competing financial interests or personal relationships that could have appeared to influence the work reported in this paper.

## Acknowledgments

The authors would like to thank Prof. Dr. Z. Hassan, the director of INOR-USM in Malaysia, for his support of this work, as well as all members of the INOR technical team who have effectively maintained all measurements.

## References

[1] A.M. Selman, Synthesis and characterization of GaN nanocrystalline thin films on various substrates by RF magnetron sputtering, Exp. Theor. Nanotechnol. 4 (May) (2020) 35–40 [Online]. Available: http://www.siats.co.uk/wp-content/files_mf/etn/040104.pdf.

[2] C. Ngom, et al., Modelling of charge injection by multi-photon absorption in GaN-on-Si HEMTs for SEE testing, in: Microelectron. Reliab, 126, 2021, 114339, https://doi.org/10.1016/j.microrel.2021.114339.

[3] N.B. Uner, E. Thimsen, Nonequilibrium plasma aerotaxy of size controlled GaN nanocrystals, J. Phys. D. Appl. Phys. 53 (9) (2020), https://doi.org/10.1088/1361-6463/ab59e6.

[4] S.A. Jewett, M.S. Makowski, B. Andrews, M.J. Manfra, A. Ivanisevic, Gallium nitride is biocompatible and non-toxic before and after functionalization with peptides, Acta Biomater. 8 (2) (2012) 728–733, https://doi.org/10.1016/j.actbio.2011.09.038.

[5] C.M. Foster, R. Collazo, Z. Sitar, A. Ivanisevic, Aqueous stability of Ga- and N-polar gallium nitride, Langmuir 9 (1) (2013) 216–220, https://doi.org/10.1021/la304039n.

[6] H. Zhang, Y. Chen, L. Fu, J. Ma, Synthesis, thermal stability, and photocatalytic activity of nanocrystalline gallium nitride via the reaction of Ga 2 O 3 and NH 4 Cl at low temperature, J. Alloy. Compd. 499 (2) (2010) 269–272, https://doi.org/10.1016/j.jallcom.2010.03.185.

[7] V. Goyal, A.V. Sumant, D. Teweldebrhan, A.A. Balandin, Direct low-temperature integration of nanocrystalline diamond with GaN substrates for improved thermal management of high-power electronics, Adv. Funct. Mater. 22 (2012) 1525–1530, https://doi.org/10.1002/adfm.201102786.

[8] J. Sung, S. Park, H. So, Cube-shaped GaN UV photodetectors using 3D-printed panels for omnidirectional detection, IEEE Sens. J. 21 (15) (2021) 16403–16408, https://doi.org/10.1109/JSEN.2021.3080506.

[9] Q.N. Abdullah, F.K. Yam, J.J. Hassan, C.W. Chin, Z. Hassan, M. Bououdina, High performance room temperature GaN-nanowires hydrogen gas sensor fabricated by chemical vapor deposition (CVD) technique, Int. J. Hydrog. Energy 38 (32) (2013) 14085–14101, https://doi.org/10.1016/j.ijhydene.2013.08.014.

[10] C.Y. Fong, S.S. Ng, F.K. Yam, H.A. Hassan, Z. Hassan, Growth of GaN on sputtered GaN buffer layer via low cost and simplified sol-gel spin coating method, Vacuum 119 (2015) 119–122, https://doi.org/10.1016/j.vacuum.2015.04.042.

[11] S. Zhang, et al., High responsivity GaN nanowire UVA photodetector synthesized by hydride vapor phase epitaxy, J. Appl. Phys. 128 (15) (2020), 155705, https://doi.org/10.1063/5.0024126.

[12] H.P. Zhang, et al., Study on the effects of growth rate on GaN films properties grown by plasma-assisted molecular beam epitaxy, J. Cryst. Growth 535 (February) (2020), 125539, https://doi.org/10.1016/j.jcrysgro.2020.125539.

[13] C.Y. Fong, S.S. Ng, F.K. Yam, H. Abu Hassan, Z. Hassan, Synthesis of two-dimensional gallium nitride via spin coating method: influences of nitridation temperatures, J. Sol. -Gel Sci. Technol. 68 (1) (2013) 95–101, https://doi.org/10.1007/s10971-013-3139-x.

[14] J.M. Lee, B.G. Min, C.W. Ju, H.K. Ahn, J.W. Lim, High temperature storage test and its effect on the thermal stability and electrical characteristics of AlGaN/GaN high electron mobility transistors, Curr. Appl. Phys. 17 (2) (2017) 157–161, https://doi.org/10.1016/j.cap.2016.11.014.

[15] D.W. Kang, J.Y. Kwon, J. Shim, H.M. Lee, M.K. Han, Highly conductive GaN anti-reflection layer at transparent conducting oxide/Si interface for silicon thin film solar cells, Sol. Energy Mater. Sol. Cells 105 (2012) 317–321, https://doi.org/10.1016/j.solmat.2012.06.041.

[16] M.R. Khan, et al., Design and characterization of GaN p-i-n diodes for betavoltaic devices, Solid. State Electron. 136 (2017) 24–29, https://doi.org/10.1016/j.sse.2017.06.010.

[17] Z. Xing, R.X. Wang, Y.M. Fan, J.F. Wang, B.S. Zhang, K. Xu, The effect of transparent conductive nanocrystalline oxide thin layer on performance of UV detectors fabricated on Fe-doped GaN, Mater. Sci. Semicond. Process. 57 (August 2016) (2017) 132–136, https://doi.org/10.1016/j.mssp.2016.10.017.

[18] J.H. Lin, S.J. Huang, Y.K. Su, K.W. Huang, The improvement of GaN-based LED grown on concave nano-pattern sapphire substrate with SiO 2 blocking layer, Appl. Surf. Sci. 354 (2015) 168–172, https://doi.org/10.1016/j.apsusc.2015.02.151.

[19] G. Devaraju, A.P. Pathak, N. Srinivasa Rao, V. Saikiran, S.V.S. Nageswara Rao, A.I. Titov, Synthesis and tailoring of GaN nanocrystals at room temperature by RF magnetron sputtering, Radiat. Eff. Defects Solids 167 (9) (2012) 659–665, https://doi.org/10.1080/10420150.2012.688204.

[20] S.H. Abud, A.M. Selman, Z. Hassan, Investigation of structural and optical properties of GaN on flat and porous silicon, Superlattices Micro 97 (2016) 586–590, https://doi.org/10.1016/j.spmi.2016.07.017.

[21] A.M. Selman, Z. Hassan, M. Husham, Structural and photoluminescence studies of rutile TiO2 nanorods prepared by chemical bath deposition method on Si substrates at different pH values, Measurement 56 (2014) 155–162.

[22] Q.N. Abdullah, et al., One-dimensional GaN nanostructures prepared via chemical vapor deposition: substrate induced size and dimensionality (PART A), Ceram. Int. 40 (7) (2014) 9563–9569, https://doi.org/10.1016/j.ceramint.2014.02.031.

[23] A. Mantarcı, M. Kundakçi, Production of GaN/n–Si thin films using RF magnetron sputtering and determination of some physical properties: argon flow impacts, J. Aust. Ceram. Soc. 56 (3) (2020) 905–914, https://doi.org/10.1007/s41779-019-00420-9.

[24] S.M. Thahab, Surface morphology effect on the optical properties of III-nitrides nanostructures for photo-sensing applications, Sens. Lett. 16 (1) (2018) 76–79, https://doi.org/10.1166/sl.2018.3908.

[25] X. Wei, R. Zhao, M. Shao, X. Xu, J. Huang, Fabrication and properties of ZnO/GaN heterostructure nanocolumnar thin film on Si (111) substrate, Nanoscale Res. Lett. 8 (1) (2013) 1–7, https://doi.org/10.1186/1556-276X-8-112.

[26] E. Li, S. Song, D. Ma, N. Fu, Y. Zhang, Synthesis and field emission properties of helical GaN nanowires, J. Electron. Mater. 43 (5) (2014) 1379–1383, https://doi.org/10.1007/s11664-014-3079-4.

[27] W.S. Liu, Y.L. Chang, H.Y. Chen, Growth of GaN thin film on amorphous glass substrate by direct-current pulse sputtering deposition technique, Coatings 9 (7) (2019) 419, https://doi.org/10.3390/COATINGS9070419.

[28] K.-C. Shen, et al., Pulsed laser deposition of hexagonal GaN-on-Si(100) template for MOCVD applications, Opt. Express 21 (22) (2013) 26468, https://doi.org/10.1364/oe.21.026468.

[29] M. Gopalakrishnan, V. Purushothaman, P.S. Venkatesh, V. Ramakrishnan, K. Jeganathan, Structural and optical properties of GaN and InGaN nanoparticles by chemical co-precipitation method, Mater. Res. Bull. 47 (11) (2012) 3323–3329, https://doi.org/10.1016/j.materresbull.2012.07.031.

[30] M. Seon, T. Prokofyeva, M. Holtz, S.A. Nikishin, N.N. Faleev, H. Temkin, Selective growth of high quality GaN on Si(111) substrates, Appl. Phys. Lett. 76 (14) (2000) 1842–1844, https://doi.org/10.1063/1.126186.

[31] K.Y. Zang, S.J. Chua, C.V. Thompson, L.S. Wang, S. Tripathy, S.Y. Chow, The effect of periodic silane burst on the properties of GaN on Si (111) substrates, Mater. Res. Soc. Symp. Proc. 831 (111) (2005) 1–6.

[32] K.M.A. Saron, et al., Leakage current reduction in n-GaN/p-Si (100) heterojunction solar cells, Appl. Phys. Lett. 118 (2) (2021), https://doi.org/10.1063/5.0037866.

[33] A. Bittar, H.J. Trodahl, N.T. Kemp, A. Markwitz, Ion-assisted deposition of amorphous GaN: Raman and optical properties, Appl. Phys. Lett. 78 (5) (2001) 619–621, https://doi.org/10.1063/1.1345800.

[34] M.J. Kadhim, M.A. Mahdi, J.J. Hassan, Influence of pH on the photocatalytic activity of ZnO nanorods, Mater. Int 2 (2) (2020) 0064–0072, https://doi.org/10.1007/s10854-016-4284-0.

[35] M.A. Mahdi, Z. Hassan, S.S. Ng, J.J. Hassan, S.K.M. Bakhori, Structural and optical properties of nanocrystalline CdS thin films prepared using microwave-assisted chemical bath deposition, Thin Solid Films 520 (9) (2012) 3477–3484, https://doi.org/10.1016/j.tsf.2011.12.059.

[36] B. Duan, Z. Wang, X. Li, Defect-related photoluminescence of gallium nitride / silicon nanoporous pillar array modulated by ammonia gas flow rate, Mater. Sci. Semicond. Process. 123 (January) (2020), 105473, https://doi.org/10.1016/j.mssp.2020.105473.

[37] A.M. El-Naggar, Effect of thickness on the structural and optical properties of GaN films grown on Si(111), J. Mater. Sci. Mater. Electron 23 (4) (2012) 972–976, https://doi.org/10.1007/s10854-011-0529-0.

[38] H. So, W. Park, Attachable freezing-delayed surfaces for ultraviolet sensing using GaN photodetector at low temperature in air, Appl. Surf. Sci. 473 (2019) 261–265, https://doi.org/10.1016/j.apsusc.2018.11.196.

[39] A.M. Selman, Z. Hassan, Fabrication and characterization of metal-semiconductor-metal ultraviolet photodetector based on rutile TiO2 nanorod, Mater. Res. Bull. 73 (2016) 29–37, https://doi.org/10.1016/j.materresbull.2015.08.013.

[40] Q.N. Abdullah, et al., Growth and characterization of GaN nanostructures under various ammoniating time with fabricated Schottky gas sensor based on Si substrate, Superlattices Micro 117 (2018) 92–104, https://doi.org/10.1016/j.spmi.2018.02.011.

[41] H. Wang, et al., Optimization of all figure-of-merits in well-aligned GaN microwire array based Schottky UV photodetectors by Si doping, ACS Photonics 6 (2019) 1972–1980, https://doi.org/10.1021/acsphotonics.9b00363.

[42] S. Krishna, et al., Correlation of donor-acceptor pair emission on the performance of GaN-based UV photodetector, 2019, Mater. Sci. Semicond. Process. 98 (July) (2018) 59–64, https://doi.org/10.1016/j.mssp.2019.03.009.

[43] A.M. Selman, M.A. Mahdi, Z. Hassan, Fabrication of Cu2O nanocrystalline thin films photosensor prepared by RF sputtering technique, Phys. E Low. -Dimens. Syst. Nanostruct. 94 (June) (2017) 132–138, https://doi.org/10.1016/j.physe.2017.08.007.

[44] A.M. Selman, Z. Hassan, M. Husham, N.M. Ahmed, A high-sensitivity, fast-response, rapid-recovery p–n heterojunction photodiode based on rutile TiO2 nanorod array on p-Si(1 1 1), Appl. Surf. Sci. jou vol. 305 (2014) 445–452.

[45] N. Prakash, et al., Ultrasensitive self-powered large area planar GaN UV-photodetector using reduced graphene oxide electrodes, Appl. Phys. Lett. 109 (24) (2016), 242102, https://doi.org/10.1063/1.4971982.

[46] A.M. Selman, Z. Hassan, Highly sensitive fast-response UV photodiode fabricated from rutile TiO2 nanorod array on silicon substrate, Sens. Actuators, A Phys. 221 (2015) 15–21, https://doi.org/10.1016/j.sna.2014.10.041.

[47] S. Chang, M. Chang, Y. Yang, Enhanced responsivity of GaN metal-semiconductor-metal (MSM) photodetectors on GaN substrate, IEEE Photonics J. 9 (2) (2017), https://doi.org/10.1109/JPHOT.2017.2688520.

[48] D. Guo, et al., Self-powered ultraviolet photodetector with superhigh photoresponsivity (3.05 A/W) based on the GaN/Sn:Ga 2 O 3 pn junction, ACS Nano 12 (12) (2018) 12827–12835, https://doi.org/10.1021/acsnano.8b07997.

[49] X. Sun, C. Wu, Y. Wang, D. Guo, Photoinduced carrier transport mechanism in pn-and nn-GaN/GaON heterojunctions, J. Vac. Sci. Technol. B, Nanotechnol. Microelectron. Mater. Process. Meas. Phenom. 40 (1) (2022) 12204.

[50] M.A. Mahdi, J.J. Hassan, N.M. Ahmed, S.S. Ng, Z. Hassan, Growth and characterization of CdS single-crystalline micro-rod photodetector, Superlattices Micro 54 (1) (2013) 137–145, https://doi.org/10.1016/j.spmi.2012.11.005.

[51] N.K.R. Nallabala, et al., Enhanced photoresponse performance in GaN based symmetric type MSM ultraviolet-A and MIS ultraviolet-A to C photodetectors, Sens. Actuators A Phys. 339 (2022), 113502.

[52] G. Yadav, V. Gupta, M. Tomar, Double Schottky metal–semiconductor–metal based GaN photodetectors with improved response using laser MBE technique, J. Mater. Res. 37 (2022) 1–13.

[53] N. Aggarwal, et al., A highly responsive self-Driven UV photodetector using GaN nanoflowers, Adv. Electron. Mater. 3 (2017) 1–7, https://doi.org/10.1002/aelm.201700036.

[54] A.H.G. Nanowire, U.V. Photodetector, I.T. Gan, A high-responsivity GaN nanowire UV photodetector, IEEE J. Sel. Top. Quantum Electron. 17 (4) (2011) 996–1001.

[55] M. Peng, et al., Flexible self-powered gan ultraviolet photoswitch with piezo-phototronic effect enhanced on/off ratio, ACS Nano 10 (1) (2016) 1572–1579, https://doi.org/10.1021/acsnano.5b07217.